Mass measurement of ^{51}Fe for the determination of the ^{51}Fe$(p,\gamma)^{52}$Co reaction rate

W.-J. Ong,[1,2] A. A. Valverde,[3] M. Brodeur,[3] G. Bollen,[1,4] M. Eibach,[5,2] K. Gulyuz,[2] A. Hamaker,[1,2] C. Izzo,[1,2] D. Puentes,[1,2] M. Redshaw,[2,6] R. Ringle,[2] R. Sandler,[6] S. Schwarz,[2] C. S. Sumithrarachchi,[2] J. Surbrook,[1,2] A. C. C. Villari,[4] and I. T. Yandow[1,2]

[1]*Department of Physics and Astronomy, Michigan State University, East Lansing, Michigan 48824, USA*
[2]*National Superconducting Cyclotron Laboratory, East Lansing, Michigan 48824, USA*
[3]*Department of Physics, University of Notre Dame, Notre Dame, Indiana 46556, USA*
[4]*Facility for Rare Isotope Beams, East Lansing, Michigan 48824, USA*
[5]*Institut für Physik, Ernst-Moritz-Arndt-Universität, 17487 Greifswald, Germany*
[6]*Department of Physics, Central Michigan University, Mount Pleasant, Michigan 48859, USA*

(Received 25 September 2018; published 10 December 2018)

Background: The ^{51}Fe$(p,\gamma)^{52}$Co reaction lies along the main rp-process path leading up to the ^{56}Ni waiting point. The uncertainty in the reaction Q value, which determines the equilibrium between the forward proton-capture and reverse photodisintegration ^{52}Co$(\gamma,p)^{51}$Fe reaction, contributes to considerable uncertainty in the reaction rate in the temperature range of interest for Type I x-ray bursts and thus to an ≈10% uncertainty in burst ashes lighter than $A = 56$.

Purpose: With a recent Penning trap mass measurement of ^{52}Co reducing the uncertainty on its mass to 6.6 keV [Nesterenko *et al.*, J. Phys. G **44**, 065103 (2017)], the dominant source of uncertainty in the reaction Q value is now the mass of ^{51}Fe, reported in the 2016 atomic mass evaluation to a precision of 9 keV [Wang *et al.*, Chin. Phys. C **41**, 030003 (2017)]. A new, high-precision Penning trap mass measurement of ^{51}Fe was performed to allow the determination of an improved precision Q value and thus new reaction rates.

Method: ^{51}Fe was produced using projectile fragmentation at the Coupled Cyclotron Facility at the National Superconducting Cyclotron Laboratory, and separated using the A1900 fragment separator. The resulting secondary beam was then thermalized in the beam stopping area before a mass measurement was performed using the LEBIT 9.4T Penning trap mass spectrometer.

Results: The new mass excess, ME $= -40189.2(1.6)$ keV, is sixfold more precise than the current AME value, and 1.6σ less negative. This value was used to calculate a new proton separation energy for ^{52}Co of 1431(7) keV. New excitation levels were then calculated for ^{52}Co using the NUSHELLX code with the GXPF1A interaction, and a new reaction rate and burst ash composition was calculated.

Conclusions: With a new measured Q value, the uncertainty on the ^{51}Fe(p,γ) reaction rate is dominated by the poorly measured ^{52}Co level structure. Reducing this uncertainty would allow a more precise rate calculation and a better determination of the mass abundances in the burst ashes.

DOI: 10.1103/PhysRevC.98.065803

I. INTRODUCTION

Type I x-ray bursts occur due to explosive burning of H/He-rich material accreted onto a neutron star from its companion star [1]. During this event, progressively heavier elements are formed through a sequence of the 3α process, the α, p process, and finally the rapid proton capture or rp-process. In order to accurately understand the physics of x-ray bursts, as well as to glean insights regarding the properties of the host neutron star, the nuclear physics of these processes must be well known.

The rp-process is a series of proton captures and β decays that proceeds close to the proton drip line, where the properties of many of the nuclei are poorly, or completely, unknown. Recent sensitivity studies of reaction rates [2] and masses [3] demonstrate the large magnitude of variation when modeling the x-ray burst light curve and rp-process ash composition that arises due to uncertainties in nuclear quantities. There has also been a concurrent effort to measure the reaction rates and masses of nuclei that have been identified as the largest sources of uncertainty.

The reaction ^{51}Fe$(p,\gamma)^{52}$Co lies along the main rp-process path leading up to the ^{56}Ni waiting point. The current reaction rates recommended by the commonly used REACLIB reaction rate database [4] span two orders of magnitude in the temperature range of interest for x-ray bursts ($0.1 \lesssim T_9 \lesssim 3.0$), which leads to a ≈10–15 % difference in $A = 51$ burst ashes and up to ≈5% differences in mass 52–56 ashes. Existing uncertainty in the reaction Q value, which determines the conditions under which ^{51}Fe$(p,\gamma)^{52}$Co comes into equilibrium with the photodisintegration reverse reaction ^{52}Co$(\gamma,p)^{51}$Fe, also leads to a similar order of magnitude uncertainty in the burst ash composition.

To reduce this uncertainty, we report the first Penning trap mass measurement of ^{51}Fe. The current mass excess of ^{51}Fe given in the most recent atomic mass evaluation

(AME2016 [5]) is −40203(9) keV and is largely based on the most recent storage ring mass measurement of −40192(11) keV [6]. With the recent JYFLTRAP mass measurement of ^{52}Co [7] that reduced the uncertainty of the ^{52}Co mass excess to several keV, the remaining Q-value uncertainty arose from ^{51}Fe.

With the new reaction Q value and a new shell model calculation of states in ^{52}Co, we recommend new ^{51}Fe$(p,\gamma)^{52}$Co and ^{52}Co$(\gamma,p)^{51}$Fe reaction rates, investigate the impact of the new rates through single zone x-ray burst simulations, and discuss the remaining sources of uncertainty.

II. METHOD

^{51}Fe was produced at the National Superconducting Cyclotron Laboratory (NSCL) and measured at the Low-Energy Beam and Ion Trap (LEBIT) facility [8]. The LEBIT facility is unique among Penning trap mass spectrometry facilities in its ability to perform high-precision mass measurements on rare isotopes produced by projectile fragmentation. A schematic of the gas cell and LEBIT facility at the NSCL can be seen in Fig. 1. In this experiment, radioactive ^{51}Fe was produced by impinging a 160 MeV/u primary beam of ^{58}Ni on a 752 mg/cm^2 beryllium target at the Coupled Cyclotron Facility at the NSCL. The resulting beam passed through the A1900 fragment separator with a 240 mg/cm^2 aluminum wedge [9] to separate the secondary beam. This beam consisted of ^{51}Fe (11.8%), with contaminants of ^{50}Mn, ^{49}Cr, and ^{48}V.

The beam then entered the beam stopping area [10] through a momentum compression beamline, where it was degraded with aluminum degraders of 87 mg/cm^2 and 270 mg/cm^2 thickness before passing through a 275 mg/cm^2, 4.5 mrad aluminum wedge and entering the gas cell with an energy of less than 1 MeV/u. In the gas cell, ions are stopped through collisions with the high-purity helium gas at a pressure of about 73 mbar; during this process, the highly charged ions recombine down to a singly charged state. These ions were transported by a combination of RF and DC fields as well as

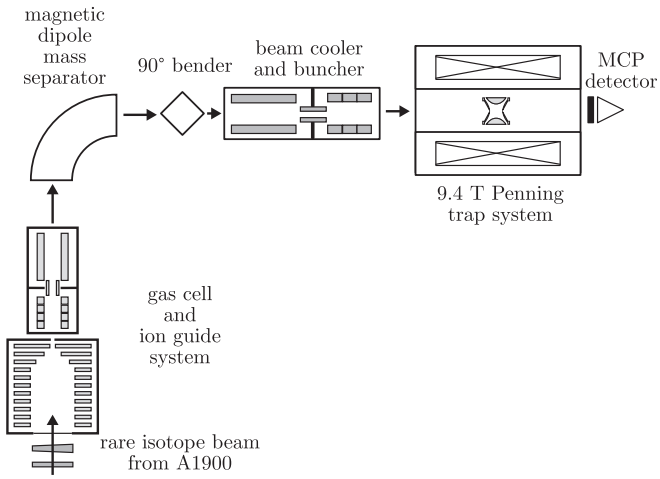

FIG. 1. A schematic diagram showing the major elements of the gas cell and LEBIT facility.

gas flow through the gas cell, and were then extracted into a radiofrequency quadrupole (RFQ) ion guide and transported through a magnetic dipole mass separator with a resolving power greater than 500. Transmitted activity after the mass filter was measured using an insertable Si detector, and confirmed to be present at $A/Q = 51$.

In the LEBIT facility, the ^{51}Fe$^+$ ions first entered the cooler-buncher, a multistaged helium-gas-filled RFQ ion trap [11]. In the first stage, moderate pressure ($\approx 10^{-3}$ mbar) helium gas was used to cool the ions in a large diameter RFQ ion guide. In the final, ions were accumulated, cooled, and released to the LEBIT Penning trap in pulses of approximately 100 ns [12]. A fast kicker in the beam line between the cooler-buncher and the Penning trap was used as a time-of-flight mass separator to further purify the beam, selecting ions of $A/Q = 51$, corresponding to ^{51}Fe$^+$ and contaminants of the same A/Q.

The 9.4T Penning trap at the LEBIT facility consists of a high-precision hyperbolic electrode system contained in an actively-shielded 9.4T magnet system [8]. Electrodes in front of the Penning trap are used to decelerate the ion pulses to low energy before entering the trap. The final section of these electrodes are quadrisected radially to form a "Lorentz steerer" [13] that forces the ions to enter the trap off-axis and perform a magnetron motion of frequency ν_- once the trapping potential is switched on.

After their capture, the trapped ions were purified, using the dipole cleaning technique [14], reducing the abundance of contaminants to less than a few percent. In this technique, azimuthal RF dipole fields are used to excite contaminant ions at their specific reduced cyclotron frequency ν_+ and thus drive them to a large enough radius such that they do not interfere with the measurement. Then, the time-of-flight cyclotron resonance technique (TOF-ICR) [15,16] was used to determine the ions' cyclotron frequency. From this resonance one can measure the cyclotron frequency $\nu_c = qB/(2\pi m)$ and so determine the mass m for a known charge q and magnetic field strength B.

In this measurement, 50 and 250 ms continuous quadrupole resonances and 125 ms Ramsey quadrupole resonances were used. In a continuous resonance, either 50 or 250 ms of continuous RF quadrupole excitation are applied in a single pulse [16]; for a Ramsey resonance, a two-pulse excitation scheme was used, where two 25 ms quadrupole RF pulses were separated by a 75 ms waiting time [17–19]. Afterwards, a fit to the theoretical line shape was performed to determine the cyclotron frequency; sample fits of both types can be seen in Fig. 2. Between measurements of ^{51}Fe$^+$, measurements of the cyclotron frequency of the reference chloromethyl ion, ^{12}C^{1}H$_2$^{37}Cl$^+$, were taken. The chloromethyl was produced in the gas cell.

III. RESULTS

A. New mass excess of ^{51}Fe

In Penning trap mass spectrometry, the experimental result is the ratio $R = \nu_{\mathrm{ref}}^{\mathrm{int}}(\mathrm{CH_2Cl^+})/\nu_c(^{51}\mathrm{Fe}^+)$, where in this case, $\nu_{\mathrm{ref}}^{\mathrm{int}}$ is the interpolated frequency of the chloromethyl reference

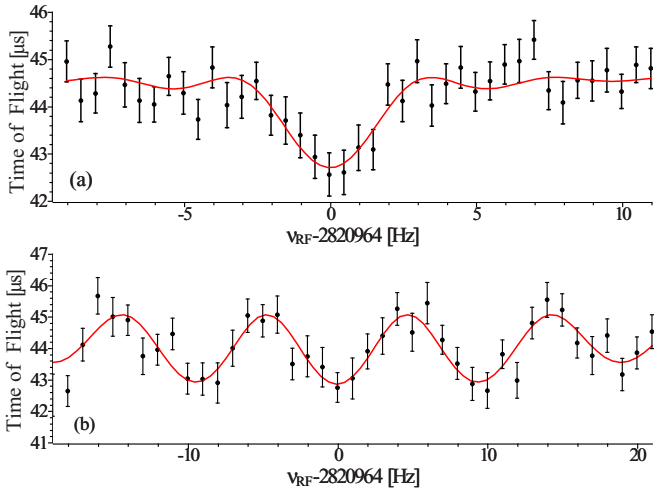

FIG. 2. A sample 250-ms $^{51}Fe^{+}$ time-of-flight traditional continuous cyclotron resonance (top) and 125-ms $^{51}Fe^{+}$ time-of-flight Ramsey cyclotron resonance (bottom) used for the determination of the frequency ratio of $\nu_{\mathrm{ref}}^{\mathrm{int}}(CH_2{}^{37}Cl^{+})/\nu_c(^{51}Fe^{+})$. The solid red curves represents a fit of the theoretical profile [16,17].

ion bracketing the measurement of ν_c, the cyclotron frequency of $^{51}Fe^{+}$. A series of five measurements was taken over the course of four hours, resulting in a weighted average of $\overline{R} = 0.999515555(29)$. These measurements are shown in Fig. 3. The Birge ratio [20] of 0.54(21), less than one, indicates that the statistical uncertainties on the individual measurements has not been underestimated.

Previous work has shown that the effect of nonlinear magnetic field fluctuations on the ratio R is less than 1×10^{-9} per hour [21], longer than our measurement time. The presence of isobaric contaminants in the trap during a measurement could also lead to a systematic frequency shift [22]. This effect was minimized by ensuring no contaminants were present at a level exceeding a few percent through cleaning and by limiting the total number of ions in the trap. This was done by analyzing events with five or fewer detected ions, corresponding to eight or fewer ions in the trap based on our measured MCP efficiency of 63% [23]. Furthermore, a z-class analysis was performed, and any count-dependent systematic shifts were found to be more than an order of magnitude smaller than the statistical uncertainty. As $^{51}Fe^{+}$ and the chloromethyl ion form an isobaric doublet, most of the mass-dependent systematic shifts, such as relativistic shifts

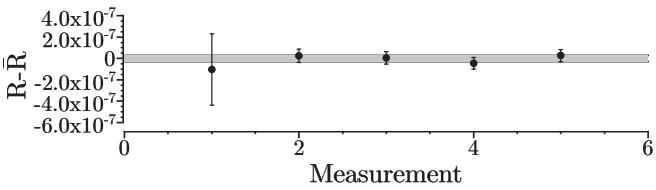

FIG. 3. Measured cyclotron frequency ratios $R = \nu_{\mathrm{ref}}^{\mathrm{int}}(CH_2{}^{37}Cl)/\nu_c(^{51}Fe)$ relative to the weighted average $\overline{R}$. The grey bar represents the 1σ uncertainty in $\overline{R}$.

TABLE I. New shell model excitation levels for ^{52}Co over the proton separation energy and up to 4 MeV. Spectroscopic factors C^2S used to calculate the partial proton and gamma widths (Γ_p and Γ_γ, respectively) were calculated utilizing the shell model with the GXPF1A interaction [29] that allowed up to three-particle–three-hole configurations. Only states above the proton separation energy are listed.

Levels (keV)			C^2S		Γ (eV)	
E_x	E_{res}	J^π	$l=1$	$l=3$	Γ_γ	Γ_p
1560	129	5^+	4.17×10^{-2}	4.17×10^{-2}	8.26×10^{-4}	4.12×10^{-20}
1601	170	4^+	2.94×10^{-1}	2.94×10^{-1}	4.21×10^{-4}	1.32×10^{-15}
1716	285	4^+	2.28×10^{-1}	2.46×10^{-2}	1.57×10^{-4}	3.67×10^{-9}
1818	387	6^+		3.38×10^{-2}	1.84×10^{-2}	1.57×10^{-9}
1954	523	5^+		1.12×10^{-1}	1.53×10^{-2}	4.40×10^{-7}
2027	596	4^+	1.03×10^{-2}	4.26×10^{-2}	1.65×10^{-2}	2.89×10^{-5}
2047	616	3^+	9.10×10^{-3}	1.02×10^{-1}	7.18×10^{-3}	3.93×10^{-5}
2126	695	5^+		4.49×10^{-2}	8.58×10^{-3}	6.08×10^{-6}
2161	730	2^+	8.59×10^{-2}	2.10×10^{-1}	2.00×10^{-2}	3.02×10^{-3}
2262	831	3^+	5.00×10^{-4}	1.11×10^{-1}	4.25×10^{-3}	7.65×10^{-5}
2263	832	5^+		2.25×10^{-2}	6.90×10^{-3}	2.14×10^{-5}
2358	927	1^+	2.00×10^{-3}	1.27×10^{-2}	2.67×10^{-2}	9.74×10^{-4}
2415	984	6^+		5.20×10^{-3}	3.55×10^{-4}	2.55×10^{-5}
2498	1067	1^+	2.10×10^{-3}	3.00×10^{-4}	1.81×10^{-3}	4.09×10^{-3}
2521	1090	5^+		2.00×10^{-4}	5.03×10^{-3}	2.47×10^{-6}
2575	1144	2^+	3.79×10^{-2}	2.08×10^{-2}	1.51×10^{-2}	1.41×10^{-1}
2603	1172	4^+	7.70×10^{-3}	3.10×10^{-2}	2.79×10^{-3}	3.56×10^{-2}
2641	1210	3^+	2.42×10^{-2}	8.10×10^{-2}	8.16×10^{-3}	1.48×10^{-1}
2649	1218	6^+		2.50×10^{-3}	3.00×10^{-3}	7.91×10^{-5}
2667	1236	1^+	4.02×10^{-1}	3.47×10^{-2}	1.28×10^{-2}	2.97
2701	1270	4^+	1.03×10^{-2}	2.30×10^{-1}	1.78×10^{-2}	9.61×10^{-2}
2716	1285	2^+	6.55×10^{-2}	1.66×10^{-2}	1.16×10^{-2}	6.75×10^{-1}
2776	1345	2^+	1.43×10^{-2}	1.50×10^{-3}	8.05×10^{-3}	2.16×10^{-1}
2801	1370	3^+	4.41×10^{-2}	2.34×10^{-2}	2.61×10^{-2}	7.75×10^{-1}
2839	1408	3^+	4.00×10^{-4}	8.10×10^{-3}	5.30×10^{-3}	8.77×10^{-3}
2879	1448	0^+		6.00×10^{-4}	5.00×10^{-4}	1.65×10^{-2}
2919	1488	6^+		1.80×10^{-3}	1.23×10^{-2}	2.70×10^{-4}
2920	1489	3^+	3.30×10^{-3}	4.00×10^{-3}	2.37×10^{-3}	1.13×10^{-1}
2921	1490	0^+		8.90×10^{-3}	7.64×10^{-2}	1.34×10^{-3}
2943	1512	1^+	6.82×10^{-2}	6.70×10^{-3}	5.62×10^{-2}	2.62
2954	1523	4^+	4.20×10^{-3}	5.90×10^{-3}	6.70×10^{-3}	1.71×10^{-1}
2992	1561	6^+		5.00×10^{-4}	1.07×10^{-2}	1.05×10^{-4}
3020	1589	2^+	1.58×10^{-1}	3.10×10^{-3}	1.37×10^{-2}	8.85
3021	1590	5^+		1.10×10^{-3}	3.20×10^{-2}	2.63×10^{-3}
3032	1601	3^+	6.34×10^{-2}	1.98×10^{-2}	4.22×10^{-3}	3.76
3082	1651	2^+	1.78×10^{-2}	1.39×10^{-2}	3.25×10^{-2}	1.33
3119	1688	4^+	2.47×10^{-2}	1.80×10^{-3}	2.31×10^{-2}	2.16
3171	1740	1^+	3.74×10^{-2}	2.00×10^{-4}	6.78×10^{-4}	4.07
3172	1741	5^+		3.14×10^{-2}	1.27×10^{-2}	1.39×10^{-2}
3191	1760	3^+	4.30×10^{-3}	8.50×10^{-3}	1.22×10^{-2}	5.07×10^{-1}
3236	1805	2^+	1.29×10^{-1}	1.00×10^{-4}	7.51×10^{-2}	1.82×10^{1}
3279	1848	4^+	6.10×10^{-3}	1.06×10^{-2}	8.71×10^{-3}	1.01
3287	1856	1^+	9.01×10^{-2}	1.92×10^{-2}	7.01×10^{-2}	1.54×10^{1}
3289	1858	5^+		1.10×10^{-3}	1.06×10^{-2}	7.46×10^{-4}
3331	1900	3^+	1.60×10^{-3}	2.80×10^{-3}	1.12×10^{-2}	3.20×10^{-1}
3333	1902	2^+	8.50×10^{-3}	5.80×10^{-3}	1.60×10^{-3}	1.71
3398	1967	4^+	1.11×10^{-2}	1.26×10^{-2}	9.06×10^{-3}	2.80
3413	1982	1^+	1.17×10^{-2}	5.90×10^{-3}	1.99×10^{-3}	3.10
3427	1996	2^+	3.76×10^{-2}	4.50×10^{-3}	1.14×10^{-2}	1.04×10^{1}

TABLE I. (*Continued.*)

Levels (keV)			C^2S		Γ (eV)	
E_x	$E_{\rm res}$	J^π	$l=1$	$l=3$	Γ_γ	Γ_p
3465	2034	2^+	4.00×10^{-4}	1.30×10^{-3}	6.18×10^{-3}	1.25×10^{-1}
3503	2072	5^+		4.00×10^{-4}	1.06×10^{-2}	5.32×10^{-4}
3509	2078	3^+	1.64×10^{-2}	4.00×10^{-4}	2.51×10^{-2}	5.88
3537	2106	1^+	3.52×10^{-2}	2.19×10^{-2}	1.18×10^{-2}	1.38×10^{1}
3551	2120	3^+	3.00×10^{-3}	1.00×10^{-3}	8.66×10^{-3}	1.23
3559	2128	6^+		1.40×10^{-3}	1.52×10^{-2}	2.19×10^{-3}
3575	2144	5^+		2.30×10^{-2}	8.36×10^{-3}	3.76×10^{-2}
3576	2145	4^+	1.46×10^{-2}	5.90×10^{-3}	4.49×10^{-2}	6.42
3638	2207	5^+		2.00×10^{-3}	5.00×10^{-3}	3.87×10^{-3}
3645	2214	4^+	4.80×10^{-2}	3.49×10^{-2}	1.47×10^{-2}	2.57×10^{1}
3654	2223	1^+	4.00×10^{-4}	6.07×10^{-2}	1.28×10^{-2}	2.19×10^{-1}
3701	2270	6^+		6.00×10^{-4}	1.93×10^{-2}	1.36×10^{-3}
3708	2277	0^+		1.20×10^{-3}	7.47×10^{-3}	2.78×10^{-3}
3738	2307	5^+		2.70×10^{-3}	5.00×10^{-3}	6.72×10^{-3}
3741	2310	4^+	6.00×10^{-4}	4.80×10^{-3}	4.24×10^{-3}	4.16×10^{-1}
3747	2316	5^+		1.28×10^{-2}	5.00×10^{-3}	3.26×10^{-2}
3787	2356	2^+	2.34×10^{-2}	2.00×10^{-4}	3.63×10^{-3}	1.82×10^{1}
3793	2362	4^+	2.00×10^{-4}	2.90×10^{-2}	2.20×10^{-2}	1.58×10^{-1}
3883	2452	2^+	7.40×10^{-3}	2.50×10^{-3}	8.77×10^{-3}	7.28
3905	2474	1^+	8.90×10^{-3}	3.60×10^{-3}	5.80×10^{-3}	9.22
3905	2474	5^+		2.25×10^{-2}	5.00×10^{-3}	8.24×10^{-2}
3962	2531	6^+		1.00×10^{-4}	2.11×10^{-2}	4.14×10^{-4}
3977	2546	2^+	1.56×10^{-2}	4.52×10^{-2}	2.55×10^{-2}	1.90×10^{1}
3989	2558	6^+		5.30×10^{-3}	1.26×10^{-2}	2.32×10^{-2}

TABLE II. The median and 1σ upper and lower recommended rate as a function of temperature (GK).

T_9	$N_A\langle\sigma v\rangle$ (cm^3 mol^{-1} s^{-1})		
	1σ down	Median	1σ up
0.1	2.166×10^{-19}	2.177×10^{-17}	9.794×10^{-17}
0.2	5.233×10^{-12}	1.903×10^{-10}	7.216×10^{-10}
0.3	7.173×10^{-9}	1.836×10^{-7}	8.937×10^{-7}
0.4	6.200×10^{-7}	6.576×10^{-6}	4.235×10^{-5}
0.5	1.441×10^{-5}	6.487×10^{-5}	4.678×10^{-4}
0.6	1.400×10^{-4}	3.414×10^{-4}	2.4971×10^{-3}
0.7	7.347×10^{-4}	1.521×10^{-3}	9.193×10^{-3}
0.8	2.633×10^{-3}	5.465×10^{-3}	2.389×10^{-2}
0.9	7.566×10^{-3}	1.521×10^{-2}	4.926×10^{-2}
1	1.760×10^{-2}	3.521×10^{-2}	9.631×10^{-2}
1.5	3.048×10^{-1}	4.955×10^{-1}	8.588×10^{-1}
2	1.424	2.023	2.972
2.5	3.672	4.952	6.687
3	7.324	9.247	11.6672
3.5	13.089	15.5903	18.794
4	22.597	25.4879	29.3052
4.5	38.640	41.879	46.2883
5	65.462	68.9195	73.7616
6	174.35	178.033	183.316
7	407.85	411.636	417.132
8	842.41	846.079	851.543
9	1567.96	1571.65	1577.11
10	2684.66	2688.33	2693.03

due to differences in velocity and in orbital radii and shifts due to trap field imperfections, are eliminated; previous work at LEBIT has shown these shifts to be $\Delta R = 2\times10^{-10}$/u [24], so for sub-u differences, such shifts are negligible compared to the statistical uncertainty.

The ^{51}Fe mass was then calculated following:

$$M(^{51}\mathrm{Fe}) = \overline{R}[M(^{12}\mathrm{C}^1\mathrm{H}_2{}^{37}\mathrm{Cl}) - m_e] + m_e, \qquad (1)$$

where m_e the electron mass and $M(^{12}\mathrm{C}^1\mathrm{H}_2{}^{37}\mathrm{Cl})$ is the mass of the chloromethyl ion, calculated from AME2016. The electron ionization energies of iron and chloromethyl and the molecular binding energy of choloromethyl ion are both on the order of eVs and thus were not included as they are several orders of magnitude smaller than the statistical uncertainty of the measurement. The calculated mass excess of ^{51}Fe is $ME = -40189.2(1.6)$ keV, which is over sixfold more precise than the current AME2016 value, $ME = -40203(9)$ keV, and 1.6σ less negative [5]. With this new value, the proton separation energy of ^{52}Co, calculated with the newest ^{52}Co mass from [7], is 1431(7) keV.

B. ^{51}Fe$(p,\gamma)^{52}$Co reaction rate

The ^{51}Fe$(p,\gamma)^{52}$Co reaction rate remains uncertain. Constraints on the direct capture and resonant capture rates are weak as only a few excited states in ^{52}Co have been identified by experimental data [25]. The direct capture component does not contribute significantly at the relevant temperatures, as found in [26]. The resonant capture component that dominates the total reaction rate (in REACLIB) is currently purely based on a shell model calculation by [26], which used a modified KB3 interaction in the pf shell [27]. To update the reaction rate, taking into account the new reaction Q value, a shell model calculation using the code NUSHELLX [28] was performed. The calculation allowed up to three-particle–three-hole excitations in the pf shell on top of a closed ^{40}Ca core, using the newer GXPF1A interaction [29]. The results of the calculation, including spectroscopic factors C^2S, proton widths Γ_p, and γ widths Γ_γ, are listed in Table I.

A Monte Carlo approach [30,31] was used to estimate the uncertainty in the reaction rate based on the uncertainty in the shell model excitation energies. Each level was assumed to vary within a Gaussian distribution centered at the calculated value and with a width of 200 keV. The resultant distribution of rates for a given T_9 was sampled to obtain the 16th, 50th, and 84th percentiles, corresponding to the 1σ lower, median, and 1σ upper reaction rate. This was done for a range of temperatures between 0.1 and 10 GK to obtain the final rate uncertainty.

TABLE III. REACLIB fit coefficients for the recommended ^{51}Fe(p,γ) reaction rate.

a_0	a_1	a_2	a_3
2.835035×10^{2}	-1.32948×10^{1}	5.385909×10^{2}	-8.624735×10^{2}
a_4	a_5	a_6	
5.228219×10^{1}	-3.060584	4.138091×10^{2}	

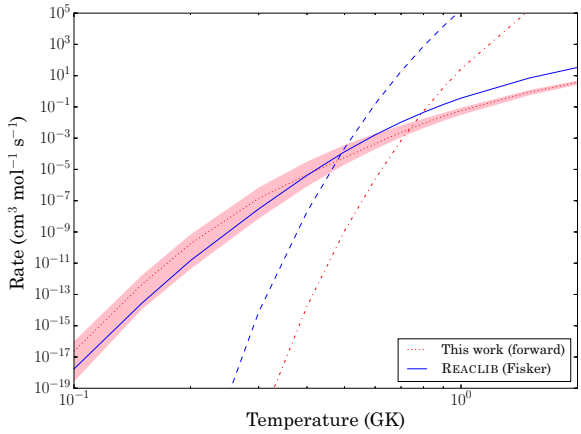

FIG. 4. Forward and reverse rates for the current recommended rate in REACLIB (blue solid and dashed, respectively) and the new recommended rate (red dotted and dot-dashed, respectively). The pale red band represents the current 1-σ uncertainty range in the reaction rate.

The new reaction rate, calculated with the new Q value taking into account the latest JYFLTRAP ^{52}Co mass result and the ^{51}Fe mass reported here, is listed for certain temperatures between 0.1–10 GK in Table II, and in the REACLIB format in Table III. A comparison with the previous reaction rate (which used a Q value of 986 keV from AME2003 [32]) is shown in Fig. 4. The impact of the higher Q value is apparent in Fig. 4, where the intersection of the forward and reverse reaction rates is ≈0.2 GK higher when compared to the current REACLIB rate. Because the ^{51}Fe(p,γ) rate is occurring close to peak temperatures of the x-ray burst, the reaction flow is particularly sensitive to where this intersection lies. The result of the higher ratio is shown in Fig. 5, where the new shell model rate (even within its 1-σ error bar) results in a faster reaction flow to higher masses, depleting the final $A = 51$ abundance and enhancing the $A = 52$–55 abundances. The enhancement in this mass region is especially important given that $A = 53$–65 nuclei are some of the biggest contributors to Urca cooling in the neutron star crust during the quiescent phase.

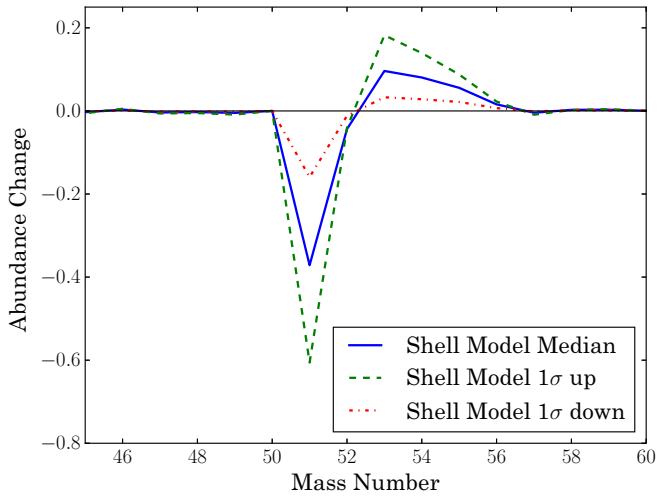

FIG. 5. Fractional differences in abundance relative to the current REACLIB rate for the median (blue solid), 1σ up (green dashed), and 1σ down (red dot-dashed) of the new reaction rate distribution.

IV. CONCLUSIONS

The first Penning trap mass measurement of ^{51}Fe was completed, producing a value with a precision of 1.6 keV, a sixfold improvement over the current AME value, which along with the recent Penning trap mass measurement of ^{52}Co allowed the calculation of the ^{52}Co proton separation to a precision of 7 keV, improving on the precision of the previous value and shifting it down by 1.3σ. Single-zone calculations incorporating the new Q value show that uncertainties of several orders of magnitude in the ^{51}Fe(p,γ) reaction rate lead to ≈10% variations in the abundances of mass 51–55 nuclei, which are some of the most abundant nuclei produced in typical x-ray bursts. However, the unknown ^{52}Co level scheme and the resultant large uncertainty in the ^{51}Fe(p,γ) reaction rate still contributes significantly to the uncertainty in the ash composition. Thus, an experimental determination of the ^{52}Co level scheme is crucial for more precise calculations of x-ray burst ashes.

Finally, constraints on the composition of x-ray burst ashes are important for observations of the cooling neutron star when it enters its quiescent phase [33]. Previous studies modeling neutron star cooling curves show that there are degeneracies between different physical properties in terms of their impact on the thermal evolution of the neutron star [34]. The impurity parameter Q that measures the inhomogeneity of the outer layers of the neutron star crust is one of the most important of these properties, and is a direct consequence of the rp-process ashes that formed the new crust. Constraints on Q would help to break these degeneracies, and provide more information about the neutron star properties, potentially including the origin of the postulated shallow heat source.

ACKNOWLEDGMENTS

The authors would like to thank Hendrik Schatz for helpful discussions regarding the rp-process calculations. This work was conducted with the support of Michigan State University, the National Science Foundation under Grants No. PHY-1102511, No. PHY-1713857, and No. PHY-1430152 (JINA Center for the Evolution of the Elements), and the U.S. Department of Energy, Office of Science, Office of Nuclear Physics under Award No. DE-SC0015927. The work leading to this publication has also been supported by a DAAD P.R.I.M.E. fellowship with funding from the German Federal Ministry of Education and Research and the People Programme (Marie Curie Actions) of the European Union's Seventh Framework Programme (FP7/2007/2013) under REA Grant Agreement No. 605728.

[1] S. E. Woosley and R. E. Taam, Nature (London) **263**, 101 (1976).

[2] R. H. Cyburt, A. M. Amthor, A. Heger, E. Johnson, L. Keek, Z. Meisel, H. Schatz, and K. Smith, Astrophys. J. **830**, 55 (2016).

[3] H. Schatz and W.-J. Ong, Astrophys. J. **844**, 139 (2017).

[4] R. H. Cyburt, A. M. Amthor, R. Ferguson, Z. Meisel, K. Smith, S. Warren, A. Heger, R. D. Hoffman, T. Rauscher, A. Sakharuk, H. Schatz, F. K. Thielemann, and M. Wiescher, Astrophys. J. **189**, 240 (2010).

[5] M. Wang, G. Audi, F. Kondev, W. Huang, S. Naimi, and X. Xu, Chin. Phys. C **41**, 030003 (2017).

[6] X. Tu, M. Wang, Y. Litvinov, Y. Zhang, H. Xu, Z. Sun, G. Audi, K. Blaum, C. Du, W. Huang, Z. Hu, P. Geng, S. Jin, L. Liu, Y. Liu, B. Mei, R. Mao, X. Ma, H. Suzuki, P. Shuai, Y. Sun, S. Tang, J. Wang, S. Wang, G. Xiao, X. Xu, J. Xia, J. Yang, R. Ye, T. Yamaguchi, X. Yan, Y. Yuan, Y. Yamaguchi, Y. Zang, H. Zhao, T. Zhao, X. Zhang, X. Zhou, and W. Zhan, Nucl. Instrum. Methods Phys. Res. A **654**, 213 (2011).

[7] D. A. Nesterenko, A. Kankainen, L. Canete, M. Block, D. Cox, T. Eronen, C. Fahlander, U. Forsberg, J. Gerl, P. Golubev, J. Hakala, A. Jokinen, V. S. Kolhinen, J. Koponen, N. Lalović, C. Lorenz, I. D. Moore, P. Papadakis, J. Reinikainen, S. Rinta-Antila, D. Rudolph, L. G. Sarmiento, A. Voss, and J. Äystö J. Phys. G: Nucl. Part. Phys. **44**, 065103 (2017).

[8] R. Ringle, G. Bollen, and S. Schwarz, Int. J. Mass Spectrom. **349–350**, 87 (2013).

[9] D. J. Morrissey, B. M. Sherrill, M. Steiner, A. Stolz, and I. Wiedenhoever, Nucl. Instrum. Methods Phys. Res. B **204**, 90 (2003).

[10] K. Cooper, C. S. Sumithrarachchi, D. J. Morrissey, A. Levand, J. A. Rodriguez, G. Savard, S. Schwarz, and B. Zabransky, Nucl. Instrum. Methods Phys. Res. A **763**, 543 (2014).

[11] S. Schwarz, G. Bollen, D. Lawton, A. Neudert, R. Ringle, P. Schury, and T. Sun, Nucl. Instrum. Methods Phys. Res. **204**, 474 (2003).

[12] R. Ringle, G. Bollen, A. Prinke, J. Savory, P. Schury, S. Schwarz, and T. Sun, Nucl. Instrum. Methods Phys. Res. A **604**, 536 (2009).

[13] R. Ringle, G. Bollen, A. Prinke, J. Savory, P. Schury, S. Schwarz, and T. Sun, Int. J. Mass Spectrom. **263**, 38 (2007).

[14] K. Blaum, D. Beck, G. Bollen, P. Delahaye, C. Guénaut, F. Herfurth, A. Kellerbauer, H.-J. Kluge, D. Lunney, S. Schwarz, L. Schweikhard, and C. Yazidjian, Europhys. Lett. **67**, 586 (2004).

[15] G. Bollen, R. B. Moore, G. Savard, and H. Stolzenberg, J. Appl. Phys. **68**, 4355 (1990).

[16] M. König, G. Bollen, H.-J. Kluge, T. Otto, and J. Szerypo, Int. J. Mass Spectrom. **142**, 95 (1995).

[17] M. Kretzschmar, Int. J. Mass Spectrom. **264**, 122 (2007).

[18] G. Bollen, H.-J. Kluge, T. Otto, G. Savard, and H. Stolzenberg, Nucl. Instrum. Methods Phys. Res. B **70**, 490 (1992).

[19] S. George, K. Blaum, F. Herfurth, A. Herlert, M. Kretzschmar, S. Nagy, S. Schwarz, L. Schweikhard, and C. Yazidjian, Int. J. Mass Spectrom. **264**, 110 (2007).

[20] R. T. Birge, Phys. Rev. **40**, 207 (1932).

[21] R. Ringle, T. Sun, G. Bollen, D. Davies, M. Facina, J. Huikari, E. Kwan, D. J. Morrissey, A. Prinke, J. Savory, P. Schury, S. Schwarz, and C. S. Sumithrarachchi, Phys. Rev. C **75**, 055503 (2007).

[22] G. Bollen, H.-J. Kluge, M. König, T. Otto, G. Savard, H. Stolzenberg, R. B. Moore, G. Rouleau, G. Audi, and ISOLDE Collaboration, Phys. Rev. C. **46**, R2140 (1992).

[23] A. A. Valverde, G. Bollen, M. Brodeur, R. A. Bryce, K. Cooper, M. Eibach, K. Gulyuz, C. Izzo, D. J. Morrissey, M. Redshaw, R. Ringle, R. Sandler, S. Schwarz, C. S. Sumithrarachchi, and A. C. C. Villari, Phys. Rev. Lett. **114**, 232502 (2015).

[24] K. Gulyuz, J. Ariche, G. Bollen, S. Bustabad, M. Eibach, C. Izzo, S. J. Novario, M. Redshaw, R. Ringle, R. Sandler, S. Schwarz, and A. A. Valverde, Phys. Rev. C **91**, 055501 (2015).

[25] S. E. A. Orrigo, B. Rubio, Y. Fujita, W. Gelletly, J. Agramunt, A. Algora, P. Ascher, B. Bilgier, B. Blank, L. Cáceres, R. B. Cakirli, E. Ganioğlu, M. Gerbaux, J. Giovinazzo, S. Grévy, O. Kamalou, H. C. Kozer, L. Kucuk, T. Kurtukian-Nieto, F. Molina, L. Popescu, A. M. Rogers, G. Susoy, C. Stodel, T. Suzuki, A. Tamii, and J. C. Thomas, Phys. Rev. C **93**, 044336 (2016).

[26] J. Fisker, V. Barnard, J. Görres, K. Langanke, G. Martinéz-Pinedo, and M. Wiescher, At. Data Nucl. Data Tables **79**, 241 (2001).

[27] T. T. S. Kuo and G. E. Brown, Nucl. Phys. A **114**, 241 (1968).

[28] B. A. Brown and W. D. M. Rae, Nucl. Data Sheets **120**, 115 (2014).

[29] M. Honma, T. Otsuka, B. A. Brown, and T. Mizusaki, Eur. Phys. J. A **25**, 499 (2005).

[30] W.-J. Ong, C. Langer, F. Montes, A. Aprahamian, D. W. Bardayan, D. Bazin, B. A. Brown, J. Browne, H. Crawford, R. Cyburt, E. B. Deleeuw, C. Domingo-Pardo, A. Gade, S. George, P. Hosmer, L. Keek, A. Kontos, I.-Y. Lee, A. Lemasson, E. Lunderberg, Y. Maeda, M. Matos, Z. Meisel, S. Noji, F. M. Nunes, A. Nystrom, G. Perdikakis, J. Pereira, S. J. Quinn, F. Recchia, H. Schatz, M. Scott, K. Siegl, A. Simon, M. Smith, A. Spyrou, J. Stevens, S. R. Stroberg, D. Weisshaar, J. Wheeler, K. Wimmer, and R. G. T. Zegers, Phys. Rev. C **95**, 055806 (2017).

[31] C. Iliadis, R. Longland, A. Coc, F. X. Timmes, and A. E. Champagne, J. Phys. G: Nucl. Part. Phys. **42**, 034007 (2015).

[32] G. Audi, A. Wapstra, and C. Thibault, Nucl. Phys. A **729**, 337 (2003), the 2003 NUBASE and Atomic Mass Evaluations.

[33] H. Schatz, S. Gupta, P. Möller, M. Beard, E. F. Brown, A. T. Deibel, L. R. Gasques, W. R. Hix, L. Keek, R. Lau, A. W. Steiner, and M. Wiescher, Nature (London) **505**, 62 (2014).

[34] Z. Meisel and A. Deibel, Astrophys. J. **837**, 73 (2017).